Inorg. Chem. **2005**, *44*, 658–665

New Amine-Templated Zinc Phosphates with a Temperature-Induced Increase of Structural Dimensionality

Torben R. Jensen,*,† Nicolas Gérentes,† Josua Jepsen,‡ Rita G. Hazell,‡ and Hans J. Jakobsen§

Interdisciplinary Nanoscience Center (iNANO), Department of Chemistry, the Department of Chemistry, and Instrument Centre for Solid-State NMR Spectroscopy, Department of Chemistry, University of Aarhus, DK-8000 Århus C, Denmark

Received June 29, 2004

Three new amine-templated zinc phosphates, $[C_4N_2H_{14}][Zn(HPO_4)_2]\cdot H_2O$, **AU-I**, $[C_4N_2H_{14}][Zn_2(H_{0.5}PO_4)_2(H_2PO_4)]$, **AU-II**, and $[C_4N_2H_{14}][Zn_5(H_2O)(PO_4)_4]$, **AU-III**, are prepared by hydrothermal synthesis using an organic amine, *N*,*N*′-dimethylethylendiamine $CH_3NHCH_2CH_2NHCH_3$, as structure-directing agent. The three materials are prepared from the same reaction mixture, $1Zn(CH_3CO_2)_2{:}3.05H_3PO_4{:}2.25CH_3NHCH_2CH_2NHCH_3{:}138H_2O$ (pH = 5.1), **AU-I** at RT, **AU-II** at 60 °C, and **AU-III** at 170 °C. The materials are built from corner-sharing ZnO_4 and PO_4 tetrahedra forming chains, layers, or framework structures for **AU-I** to **III**, respectively, and are linked together by hydrogen bonds via the diprotonated amine ions. The complete hydrogen-bond scheme is resolved for these new compounds and reveals some interesting phenomena, for example, a hydrogen shared between two phosphate groups in **AU-II**, thereby forming $H_{0.5}PO_4$ groups. Furthermore, the water molecules are different; that is, in **AU–I** they act as hydrogen-bond donor and acceptor, whereas they act as ligand in **AU-III** with coordination to Zn. The structures of the compounds are determined by single-crystal X-ray diffraction analysis. **AU-I**, $[C_4N_2H_{14}][Zn(HPO_4)_2]\cdot H_2O$, crystallizes in the triclinic space group *P*-1, $a = 8.215(2)$, $b = 8.810(3)$, $c = 8.861(3)$ Å, $\alpha = 88.001(4)°$, $\beta = 89.818(5)°$, and $\gamma = 89.773(5)°$, $Z = 2$. **AU-II**, $[C_4N_2H_{14}][Zn_2(H_{0.5}PO_4)_2(H_2PO_4)]$, is monoclinic, $P2/n$, $a = 11.7877(4)$, $b = 5.2093(2)$, $c = 12.2031(4)$ Å, $\beta = 98.198(1)°$, $Z = 2$. **AU-III**, $[C_4N_2H_{14}][Zn_5(H_2O)(PO_4)_4]$, crystallizes in the orthorhombic space group $Pna2_1$ with lattice parameters, $a = 20.723(2)$, $b = 5.2095(6)$, $c = 17.874(2)$ Å, $Z = 4$. The phase stability investigated by systematic hydrothermal synthesis is presented, and the materials are further characterized by ^{31}P solid-state MAS NMR, for example, by determination of ^{31}P chemical shift anisotropies for **AU-III**, while the thermal behavior is investigated by thermogravimetry (TG).

Introduction

Design and development of new synthetic routes for novel materials with open structures have received much attention in the past two decades. Since the first open structured aluminum phosphate was discovered in the early 1980s, an extreme variety of novel architectures are observed within phosphate chemistry.[1] Novel nanoporous materials with channels and cavities of molecular dimensions are explored intensively due to a number of potential applications, for example, in catalysis, ion-exchange, gas adsorption, etc.[2]

Considering amine-templated transition metal phosphates, the zinc phosphates have the richest structural chemistry and show a variety of materials with different structural dimensionality. The first members of this still growing family of materials were discovered in the early 1990s.[3] The inorganic moiety of these materials can form chainlike (1-D) structures,[4] layered (2-D),[5] or framework structures (3-D).[6] Interrupted three-dimensional frameworks with very large

* Author to whom correspondence should be addressed. E-mail: trj@chem.au.dk.

† iNANO.

‡ Department of Chemistry.

§ Instrument Centre for Solid-State NMR Spectroscopy.

(1) (a) Wilson, S. T.; Lok, B. M.; Messina, C. A.; Cannan, T. R.; Flanigen, E. M. *J. Am. Chem. Soc*. **1982**, *104*, 1146, (b) Gier, T. E.; Stucky, G. D. *Nature (London)* **1991**, *349*, 508. (c) Feng, P.; Bu, X.; Stucky, G. D. *Nature (London)* **1997**, *388*, 735. (d) Feng, P.; Bu, X.; Stucky, G. D. *Science* **1997**, *278*, 2080. (e) Cheetham, A. K.; Ferey, G.; Loiseau, T. *Angew. Chem., Int. Ed*. **1999**, *39*, 3268.

(2) (a) Schüth, F.; Schmidt, W. *Adv. Mater*. **2002**, *14*, 629. (b) Chen, J.; Thomas, J. M. *J. Chem. Soc., Chem. Commun.* **1994**, 603. (c) Thomas, J. M.; Raja, R.; Sankar G.; Bell, R. G. *Nature (London)* **1999**, *398*, 227.

(3) (a) Harrison, W. T. A.; Martin, T. E.; Gier, T. E.; Stucky, G. D. *J. Mater. Chem*. **1992**, *2*, 175. (b) Harrison, W. T. A.; Gier, T. E.; Moran, K. L.; Nicol, J. M.; Eckert, H.; Stucky, G. D. *Chem. Mater*. **1991**, *3*, 27.

10.1021/ic049156g CCC: $30.25
Published on Web 01/05/2005

channels, consisting of 20 or 24 tetrahedra, can also be found.[7] In some cases, several new materials are prepared with the same amine as structure-directing template, for example, the cyclic amines Dabco (1,4-diazabicyclo[2.2.2]-octane) and piperazine with high degree of symmetry and relatively high charge density, providing at least eight and seven new zinc phosphate-based materials, respectively.[3,8] The amine triethylenetetramine added five new members to this family, and these materials have one-, two-, and three-dimensional structures.[9]

Nanoporous materials are usually prepared under mild conditions as they can be considered as thermodynamically metastable, meaning that the higher is the synthesis temperature, the higher is the density of the product expected to be.[10] A well-known example is the synthesis of zeolite A performed at temperatures below ca. 100 °C. Treating the same reaction mixture or a suspension of solid zeolite A at temperatures higher than ca. 100 °C produced sodalite.[11] The term hydrothermal synthesis is restricted to temperatures higher than 100 °C and water used as solvent.[12] Solvothermal synthesis is a more general term used for syntheses with an arbitrary solvent and synthetic temperature. Furthermore, it usually implies that the nucleation and crystal growth are solution mediated by dissolving the gel with an arbitrary solvent. Information on the exact mechanism for a solvothermal synthesis is usually not accessible; while the reacting species (solid or in solution) are unknown, it can be ions, clusters of ions, or larger fragments of an amorphous gel that react. Furthermore, at elevated temperatures, the pH of the solution and the solubility of the gel-phase change as well as the autogenous pressure of the closed reaction vessel (autoklave). These secondary effects caused by increased synthetic temperatures are difficult to quantify and might influence which products are formed.

In this work, we present a series of three new materials prepared from the same reaction mixture treated at different temperatures. These materials are an interesting example of the correlation between the temperature for the synthesis and the density/structural dimensionality of the synthetic products that may be obtained.

Experimental Section

Hydrothermal Synthesis. The three new materials presented here, $[C_4N_2H_{14}][Zn(HPO_4)_2]\cdot H_2O$, **AU-I**, $[C_4N_2H_{14}][Zn_2(H_{0.5}PO_4)_2(H_2PO_4)]$, **AU-II**, and $[C_4N_2H_{14}][Zn_5(H_2O)(PO_4)_4]$, **AU-III**, have been prepared from the same reaction mixture. Zinc acetate dihydrate, $Zn(CH_3CO_2)_2\cdot 2H_2O$ (6.875 g), was dissolved in water (50 mL). *N*,*N*′-Dimethylethylenediamine, $CH_3NH(CH_2)_2NHCH_3$ *dmen* (8.0 mL), was added with stirring followed by addition of H_3PO_4, 85% (11.009 g), diluted with water (25 mL), giving a molar ratio of the reactants $1Zn(CH_3CO_2)_2$:$3.05H_3PO_4$:2.25*dmen*:$138H_2O$, pH = 5.1 (measured 30 min after mixing) at RT. A portion of the gel was left at room temperature (ca. 21 °C), and another portion was kept at 60 °C, both in closed glass bottles to avoid evaporation. The remaining reaction mixture was divided into four portions, and each was heated at 100, 170, 200, and 220 °C for 24 h, respectively, in Teflon-lined steel autoclaves. After a few days, crystallization was noticed in the brown gel, both at RT and at 60 °C, and crystalline material formed after approximately 1−2 weeks at 60 °C and 6−8 weeks at R*T*. After that time, crystallization apparently stopped and the products were washed with water, recovered using vacuum filtration, and dried under ambient conditions. Powder X-ray diffraction (PXD) patterns and data from thermogravimetric (TG) measurements are available as Supporting Information (Figures S1 and S2).

Systematic syntheses were performed in a similar way as described above to investigate the crystallization fields of the different materials formed in the system $1Zn(CH_3CO_2)_2$:nH_3PO_4:2.25*dmen*:$\sim 140H_2O$ using different amounts of H_3PO_4 and a fixed temperature in the range 20−220 °C, $2.08 < n < 4.54$, giving pH in the range 3.3−6.8. The synthetic products are presented as a phase stability diagram, Figure 1.

The syntheses were performed using the following commercial chemicals: zinc acetate dihydrate, $Zn(CH_3CO_2)_2\cdot 2H_2O$ (Fluka, 99%); orthophosphoric acid, H_3PO_4 (85%, Fluka, extra pure); *N*,*N*′-dimethylethylenediamine, $CH_3NH(CH_2)_2NHCH_3$ (Lancaster, 95%).

Single-Crystal Diffraction and Structure Determination. Data collection was performed with a Siemens SMART diffractometer equipped with a CCD detector and graphite-monochromatized Mo Kα radiation (λ = 0.71073 Å).[13] Data were collected at RT in frames covering 0.3° in ω in three sets with different φ angles covering most of a hemisphere. The detector to crystal distance was 40.0 mm. Experimental details for the data collection are given in Table 1. Absorption correction was made using Gaussian integration for **AU-I** and **-II**.[13] An empirical absorption correction

(4) (a) Harrison, W. T. A.; Phillips, M. L. F. *Chem. Mater*. **1997**, *9*, 1837. (b) Harrison, W. T. A.; Bricsak, Z.; Hannooman, L.; Zhang, Z. *J. Solid State Chem*. **1998**, *136*, 93. (c) Rao, C. N. R.; Natarajan, S.; Neeraj, S. *J. Am. Chem. Soc*. **2000**, *122*, 2810. (d) Chidambaram, D.; Neeraj, S.; Natarajan, S.; Rao, C. N. R. *J. Solid State Chem*. **1999**, *147*, 154.

(5) (a) Neeraj, S.; Natarajan, S.; Rao, C. N. R. *Chem. Mater*. **1999**, *11*, 1390. (b) Neeraj, S.; Natarajan, S. *Int. J. Inorg. Mater*. **1999**, *1*, 317. (c) Harrison, W. T. A.; Bricsak, Z.; Hannooman, L. *J. Solid State Chem*. **1997**, *134*, 148. (d) Natarajan, S.; Attfield, M. P.; Cheetham, A. K. *J. Solid State Chem*. **1997**, *132*, 229.

(6) (a) Feng, P.; Bu, X.; Stucky, G. D. *Angew. Chem., Int. Ed. Engl*. **1995**, *34*, 1745. (b) Harrison, W. T. A.; Hannooman, L. *Angew. Chem., Int. Ed. Engl*. **1997**, *36*, 640. (c) Kongshaug, K. O.; Fjellvåg, H.; Lillerud, K. P. *J. Mater. Chem*. **1999**, *9*, 3119.

(7) (a) Rodgers, J. A.; Harrison, T. A. *J. Mater. Chem*. **2000**, *10*, 2853. (b) Yang, G. Y.; Slavi, C. S. *J. Am. Chem. Soc*. **1999**, *121*, 8389.

(8) (a) Feng, P.; Bu, X.; Stucky, G. D. *Angew. Chem., Int. Ed. Engl*. **1995**, *34*, 1745. (b) Patarin, J.; Marler, B.; Huve, L. *Eur. J. Solid State Inorg. Chem*. **1994**, *31*, 909−920. (c) Wallau, M.; Patarin, J.; Widmer, I.; Caullet, P.; Guth J. L.; Huve, L. *Zeolites* **1994**, *14*, 402. (d) Chavez, A. V.; Nenoff, T. M.; Hannoonman, L.; Harrison, W. T. A. *J. Solid State Chem*. **1999**, *147*, 584. (e) Ahmadi, K.; Hardy, A.; Patarin, J.; Huve, L. *Eur. J. Solid State Inorg. Chem*. **1995**, *32*, 209. (f) Neeraj, S.; Natarajan, S.; Rao, C. N. R. *Angew. Chem., Int. Ed*. **1999**, *38*, 3480. (g) Chidambaram, D.; Neeraj, S.; Natarajan, S.; Rao, C. N. R. *J. Solid State Chem*. **1999**, *147*, 154.

(9) (a) Choudhury, A.; Natarajan S.; Rao, C. N. R. *Inorg. Chem*. **2000**, *39*, 4295. (b) Liu, W.; Liu, Y.; Shi, Z.; Pang, W. *J. Mater. Chem*. **2000**, *10*, 1451. (c) Neeraj, S.; Natarajan, S.; Rao, C. N. R. *J. Solid State Chem*. **2000**, *150*, 417.

(10) Francis, R. J.; O'Hare, D. *J. Chem. Soc., Dalton Trans*. **1998**, 3133.

(11) Zeolite A (structure type, LTA) and sodalite (SOD) have framework densities of 14.2 and 16.7 tetrahedrally coordinated framework (*T*) atoms per 1000 Å^3. LTA has a three-dimensional channel system with ring sizes of 8, 6, and 4 *T* atoms, whereas SOD has a a zero-dimensional channel system with ring sizes of 6 and 4 *T* atoms. Reference: (a) Baerlocher, Ch., Meier, W. M., Olson, D. H., Eds. *Atlas of Zeolitic structure types*; Elsevier: London, 2001. (b) http://www.iza-online.org/.

(12) (a) West, A. R. *Solid State Chemistry and its Applications*; John Wiley and Sons Ltd.: Chichester, 1984; p 41. (b) Barrer, R. M. *Hydrothermal Chemistry of Zeolites*; Academic Press: London, 1982.

(13) *Siemens 1995 SMART, SAINT and XPREP Area-Detector Control and Integration Software*; Siemens Analytical X-ray Instruments Inc.: Madison, WI, 1995.

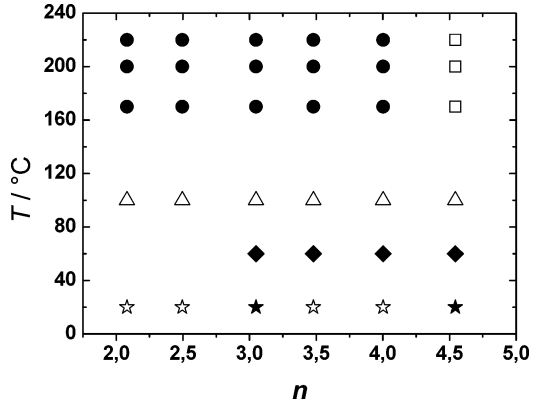

Figure 1. The crystallization fields of zinc orthophosphates formed in the system, $1Zn(CH_3CO_2)_2$:nH_3PO_4:2.25*dmen*:~$140H_2O$, at varying amounts of phosphoric acid, *n*, and temperature investigated by systematic hydrothermal synthesis. A chainlike structure $[C_4N_2H_{14}][Zn(HPO_4)_2]\cdot H_2O$, **AU-I**, was observed close to room temperature; see star symbols. A ★ symbol indicates slightly faster crystallization of **AU-I** (ca. 5 weeks) as compared to the usual crystallization time of up to 8 weeks (☆). $[C_4N_2H_{14}][Zn_2(H_{0.5}PO_4)_2(H_2PO_4)]$, **AU-II** (◆), is observed at ca. 60 °C. An unidentified white powder is indicated by △. $[C_4N_2H_{14}][Zn_5(H_2O)(PO_4)_4]$, **AU-III** (●), is obtained at relatively high temperatures, but decreasing pH (high values of *n*) tends to give hopeite, $Zn_3(PO_4)_2\cdot 4H_2O$ (□).

Table 1. Crystal Data and Structure Refinement Parameters for $[C_4N_2H_{14}][Zn(HPO_4)_2]\cdot H_2O$, **AU-I**, $[C_4N_2H_{14}][Zn_2(H_{0.5}PO_4)_2(H_2PO_4)]$, **AU-II**, and $[C_4N_2H_{14}][Zn_5(H_2O)(PO_4)_4]$, **AU-III**[a]

	AU-I	AU-II	AU-III
empirical formula	$C_4H_{18}N_2O_9P_2Zn$	$C_4H_{17}N_2O_{12}P_3Zn_2$	$C_4H_{16}N_2O_{17}P_4Zn_5$
fw	365.53	508.89	814.91
T (K)	295	295	295
space group	$P\bar{1}$ (No. 2)	$P2/n$ (No. 13)	$Pna2_1$ (No. 33)
a/Å	8.215(2)	11.7877(4)	20.723(2)
b/Å	8.810(3)	5.2093(2)	5.2095(6)
c/Å	8.861(3)	12.2031(4)	17.8741(19)
α/deg	88.001(4)	90	90
β/deg	89.818(5)	98.1980(10)	90
γ/deg	89.773(5)	90	90
V/Å^3	640.9(3)	741.68(5)	1929.6(4)
Z	2	2	4
D_{calc}/(g cm^{-3})	1.894	2.278	2.805
μ/mm^{-1}	2.206	3.623	6.548
$R(F_o^2)$[a] $[F_o^2 > 2\sigma(F_o^2)]$	0.0326	0.0267	0.0341
$R_w(F_o^2)$[a] $[F_o^2 > 2\sigma(F_o^2)]$	0.0874	0.0730	0.0661

[a] **AU-I**: $w = 1/[\sigma^2(F_o^2) + (0.0488P)^2 + 0.5666P]$, where $P = (F_o^2 + 2F_c^2)/3$. **AU-II**: $w = 1/[\sigma^2(F_o^2) + (0.0486P)^2 + 0.3967P]$, where $P = (F_o^2 + 2F_c^2)/3$. **AU-III**: $w = 1/[\sigma^2(F_o^2) + (0.0276P)^2 + 1.3880P]$, where $P = (F_o^2 + 2F_c^2)/3$.

based on symmetry-equivalent reflections was performed with the program SADABS for **AU-III**.[14] Direct methods and the programs SIR97 (**AU-I**) and SHELXS-97 (**AU-II** and **-III**) were used for the initial structural solution, and the structural models were further refined with SHELXL-97.[15,16] All hydrogen atoms on carbon in the organic moiety were placed on calculated positions, whereas hydrogen atoms participating in hydrogen bonding coordinated to nitrogen or oxygen were located in the difference Fourier maps. A

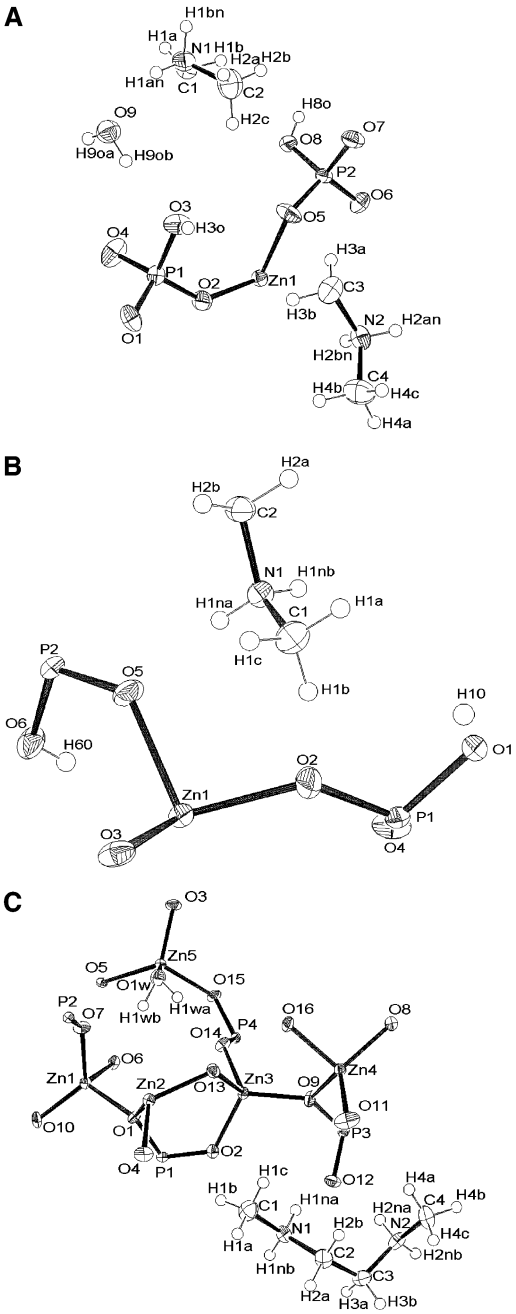

Figure 2. ORTEP style drawings showing the 50% probability thermal ellipsoids and the atom labeling for (A) $[C_4N_2H_{14}][Zn(HPO_4)_2]\cdot H_2O$, **AU-I**, (B) $[C_4N_2H_{14}][Zn_2(H_{0.5}PO_4)_2(H_2PO_4)]$, **AU-II**, and (C) $[C_4N_2H_{14}][Zn_5(H_2O)(PO_4)_4]$, **AU-III**, all in (010)-projection.

difference Fourier map for **AU-II** revealed hydrogen positions close to O1 and O6. That on O6 points toward O3, and that on O1 points toward a symmetry-related O1, disordered between two symmetry-related positions. Figure 2A−C shows ORTEP style drawings with 50% probability thermal ellipsoids and atom labeling.[17] Drawings of the crystal structures were prepared using the program Atoms Ver. 5.0.[18]

Spectroscopic Investigation. Solid-state ^{31}P CP/MAS NMR spectra were recorded at 161.8 MHz on a Varian INOVA-400 (9.4 T) spectrometer using a home-built CP/MAS probe for 5 mm o.d.

(14) Sheldrick, G. M. *SADABS Siemens Area Detector Absorption Correction Program*; University of Göttingen: Göttingen, Germany, 1994.
(15) Altomare, A.; Burla, M. C.; Camalli, M.; Cascarano, G. L.; Giacovazzo, C.; Guagliardi, A.; Moliterni, A. G. G.; Polidori, G.; Spagna, R. *J. Appl. Crystallogr*. **1999**, *32*, 115.
(16) Sheldrick, G. M. *SHELXTL*; Siemens Analytical X-ray Systems Inc.: Madison, WI, 1995.
(17) Burnett, M. N.; Johnson, C. K. ORTEP−III. Report ORNL-6895, Oak Ridge National Laboratory, TN, 1996.
(18) Dowty, E. Program ATOMS version 4.0, Shape Software, 521 hidden Valley Road, Kingsport, TN 37663, 1997.

Si_3N_4 rotors (110 μL sample volume) and a spinning speed of $\nu_R = 1800$ or 4000 Hz.[19] The ^{31}P CP/MAS experiments employed a RF field strength of $\gamma B_1/2\pi = \gamma B_2/2\pi = 40$ kHz, a pulse width of 5 μs for the first ^{1}H pulse, a relaxation delay of 16 s, and typically 2048 scans. These conditions were found to give quantitative reliable intensities in the ^{31}P CP/MAS NMR spectra. An aqueous solution of H_3PO_4 (85%, Fluka, extra pure) was used as external standard. Simulation of the solid-state ^{31}P CP/MAS NMR spectra was performed on a SUN ULTRA 5 workstation using the STARS solid-state NMR software package, developed earlier for analysis and least-squares fitting of CP/MAS or MAS NMR spectra.[20] The chemical shift anisotropy (CSA) is defined by the parameters

$$\delta_{iso} = {}^1/_3(\delta_{xx} + \delta_{yy} + \delta_{zz})$$

$$\delta_s = \delta_{iso} - \delta_{zz} \qquad \eta_\sigma = (\delta_{xx} - \delta_{yy})/\delta_\sigma \qquad (1)$$

where the principal elements of the chemical shift tensor δ_{xx}, δ_{yy}, and δ_{zz} are defined as $|\delta_{zz} - \delta_{iso}| \geq |\delta_{xx} - \delta_{iso}| \geq |\delta_{yy} - \delta_{iso}|$.

Results and Discussion

Systematic Hydrothermal Synthesis. Some new materials were prepared and initially identified by their powder diffraction profiles in this work (PXD data are available as Supporting Information, Figure S1). A number of syntheses were then performed with variation of the amount of phosphoric acid, *n*, $1Zn(CH_3CO_2)_2$:*n*H_3PO_4:2.25*dmen*:~140-H_2O, and of the synthetic temperature. The crystallization fields of the observed phases are presented in Figure 1. The one-dimensional material, $[C_4N_2H_{14}][Zn(HPO_4)_2]\cdot H_2O$, **AU-I**, crystallized only at low temperatures close to room temperature, and most of the gel was transformed to crystalline material after a relatively long time, typically 1.5−2 months (e.g., ☆ in Figure 1). However, a precursor phase (white powder) with a powder pattern similar to that of **AU-I** forms immediately (see Figure S1). The formation of **AU-I** can be observed by visual inspection of the reaction mixture placed in a closed transparent glass container. Holes were clearly visible in the white gel phase with a crystal in the bottom of each hole "eating" the gel. This phenomenon can be interpreted as dissolution of the gel followed by crystallization of **AU-I**, that is, a solution-mediated phase formation. A very similar process was observed for the transformation of gel to **AU-II** by visual inspection of the reaction mixture placed at 60 °C, but the crystallization time was only about 1 or 2 weeks. At ca. 100 °C, an unidentified material is formed but only as a white powder that has not yet been further characterized (see Figure S1). At high temperature and low pH ($n >$ ca. 4), a dense zinc phosphate, hopeite, $Zn_3(PO_4)_2\cdot 4H_2O$, is observed. Reaction mixtures with composition $2 < n < 4$ and treated at $T > 170$ °C are fully converted to phase pure samples of **AU-III** within less than 2 days. It is observed that the nucleation and crystallization time decrease as the reaction temperature is increasing for **AU-I** to **AU-III**. Notice that the crystallization of **AU-I** and **-II** apparently stopped after some time, giving a partly transformed gel as product. It was not possible to assign the resonances in the observed solid-state ^{31}P CP/MAS NMR spectra from **AU-I** and **AU-II** as these two samples are not phase pure and contain one or more unidentified phases. Therefore, only NMR data for **AU-III** are reported here.

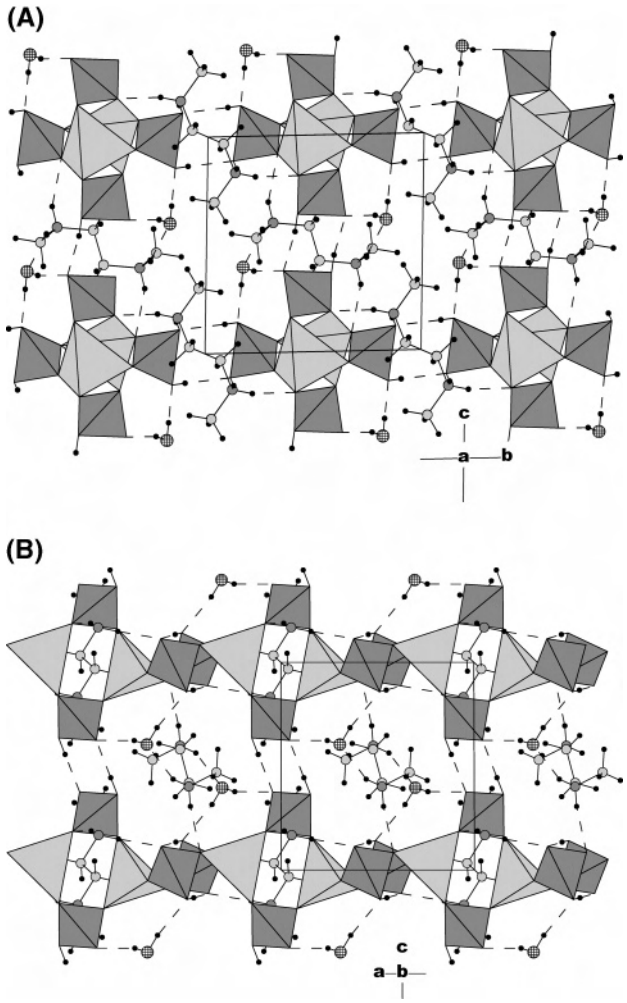

Figure 3. The crystal structure of $[C_4N_2H_{14}][Zn(HPO_4)_2]\cdot H_2O$, **AU-I**. (A) The *b*,*c*-projection, revealing a one-dimensional structure of the inorganic moiety. (B) The *a*,*c*-projection, showing chains of PO_4 and ZnO_4 tetrahedra running in the *a* direction. ZnO_4 are light and PO_4 are dark tetrahedra, water oxygens are shown as large circles with square pattern, C and N are medium size light and dark gray circles, respectively, and hydrogen are small size black circles.

Crystal Structure of $[C_4N_2H_{14}][Zn(HPO_4)_2]\cdot H_2O$, AU-I. The material $[C_4N_2H_{14}][Zn(HPO_4)_2]\cdot H_2O$, denoted **AU-I**, is triclinic and crystallizes with the symmetry *P*-1. The structure is built from regular tetrahedra of one ZnO_4 and two PO_4 in the asymmetric unit, where each phosphate has one prolonged P−O bond indicating a hydroxyl group. The ZnO_4 tetrahedra are connected to four PO_4 tetrahedra by corner sharing to form chains. Figure 3A, a *b*,*c*-projection, clearly shows that the inorganic moiety of **AU-I** forms a one-dimensional structure. Zn and P tetrahedra are connected in alternation to form four-rings connected perpendicular to each other to form a chain running along the *a* axis; see Figure 3B. These inorganic chains are similar to chains in the structure of $[C_5N_2H_{14}][Zn(HPO_4)_2]\cdot 2H_2O$.[21] Half of the

(19) Jakobsen, H. J.; Daugaard, P.; Langer, V. *J. Magn. Reson*. **1988**, *76*, 162; U.S. patent 4739270, 1988.
(20) Skibsted, J.; Nielsen, N. C.; Bildsøe, H.; Jakobsen, H. J. *J. Magn. Reson*. **1991**, *95*, 88.

diprotonated amines (*dmen*) are lying in the *a*,*b*-plane, and the other half are in the *b*,*c*-plane. The inorganic moiety, the chains, is connected by a complex hydrogen-bonding network via the organic moiety, the diprotonated amines, and water molecules. Each phosphate has two free corners participating in hydrogen bonding acting either as acceptor for two hydrogen bonds or having a dual role of both donating and accepting a hydrogen bond; see Figure 3B. The water molecule acts as donor for hydrogen bonds to the phosphate oxygens O(3) and O(7) and is acceptor for a hydrogen bond from the protonated nitrogen atom in the amine. Thereby, water and the protonated amines form a hydrogen-bond network.

Crystal Structure of $[C_4N_2H_{14}][Zn_2(H_{0.5}PO_4)_2(H_2PO_4)]$, AU-II. This new zinc ortho phosphate with composition $[C_4N_2H_{14}][Zn_2(H_{0.5}PO_4)_2(H_2PO_4)]$, denoted **AU-II**, is monoclinic and crystallizes in the space group $P2/n$. The inorganic part of the structure is built from fairly regular tetrahedra of ZnO_4 and two PO_4. One phosphorus atom, P2, is in a special position on the 2-fold rotation axis. Therefore, half the nearest oxygen (O5 and O6) and one hydrogen (H6O) are symmetry generated resulting in a H_2PO_4 group. Two refineable hydrogen positions close to O1 between the two P1 tetrahedra were observed, and based on electroneutrality of the material this is interpreted as a shared hydrogen, meaning a $H_{0.5}PO_4$ group, for the P1 tetrahedra. Therefore, the occupancy of H1O is 0.5. Figure 4A (*a*,*c*-projection) shows that **AU-II** is a layered material. Figure 4B illustrates the motif of one layer in a (101) projection. The layer consists of 4-rings and squeezed 8-rings; the latter due to phosphate P2 tetrahedra have a pendant oxygen and a hydroxyl group. The layers are stabilized by intralayer hydrogen bonding through P2−O6−H6O. Figure 4A describes the interlayer connectivity where the inorganic layers are attached to each other by hydrogen bonds through the nitrogen atom and via P1−O1−H1O···O1−P1 bridges. The diprotonated amines are placed as spacers between the layers and are oriented flat in the (101) projection; see Figure 4B.

Crystal Structure of $[C_4N_2H_{14}][Zn_5(H_2O)(PO_4)_4]$, AU-III. The formula for the new framework material $[C_4N_2H_{14}]$-$[Zn_5(H_2O)(PO_4)_4]$ is denoted **AU-III**. The primary building units are four relatively regular PO_4 tetrahedra and five slightly distorted ZnO_4 tetrahedra in the asymmetric unit forming a framework by corner sharing. One zinc tetrahedron, Zn5, has a water molecule as ligand. Figure 5A illustrates that Zn1−4 are linked together to form a secondary building unit lying parallel to the *a*-axis. These tetramers of Zn1−4 are in fact forming infinite chains by −Zn1−O−Zn2− bridges along the *b*-axis. Figure 5A is a view in the (001) direction revealing a dense network of tetrahedra. Figure 5B shows that these pseudo layers are connected to form an open framework with 10-ring channels in the *b*-axis direction containing the diprotonated amine ions. The framework is interrupted by a pendant oxygen, O(12), acting as a double hydrogen-bond acceptor for two amine protons. The diprotonated amines are lying in the *a*,*c*-plane, and both

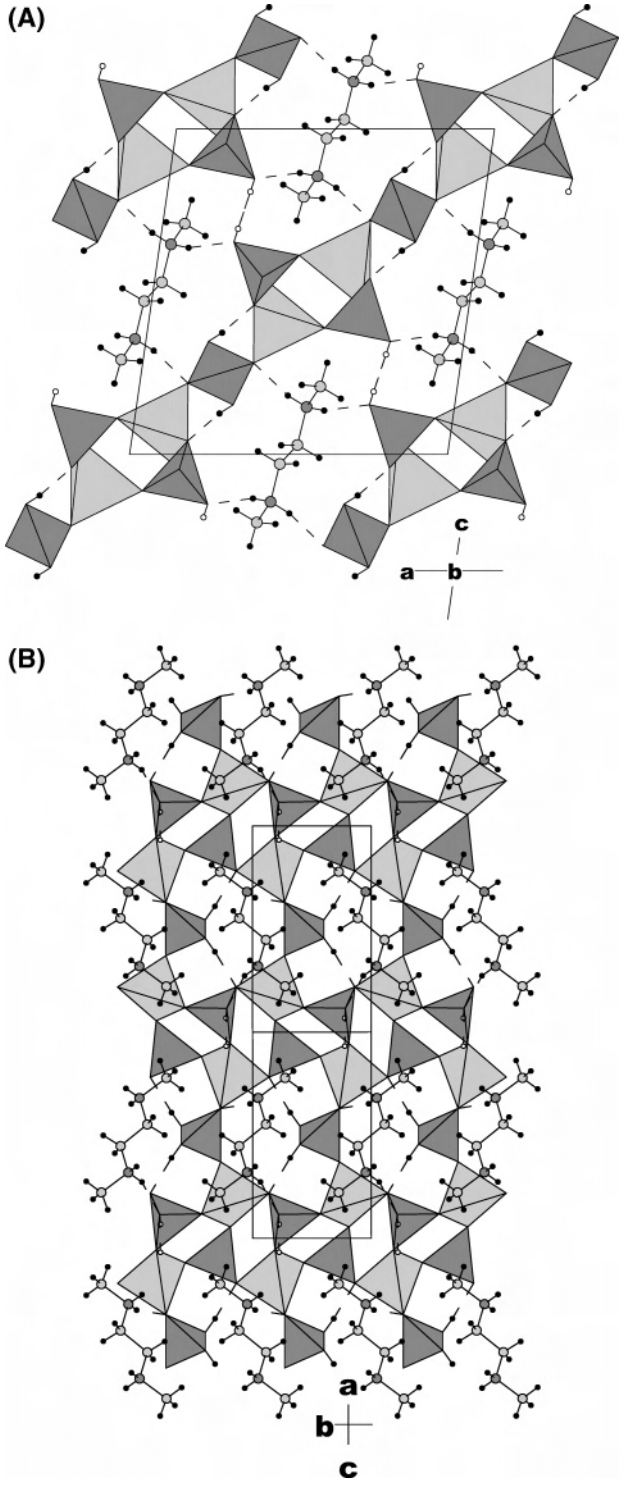

Figure 4. The crystal structure of $[C_4N_2H_{14}][Zn_2(H_{0.5}PO_4)_2(H_2PO_4)]$, **AU-II**. (A) The *a*,*c*-projection illustrating the hydrogen-bonding scheme in this layered material. (B) The (101)-projection revealing a layered structure of the inorganic moiety. ZnO_4 are light and PO_4 are dark tetrahedra, C and N are medium size light and dark gray circles, respectively, and hydrogen are small size black circles. Hydrogen, H1O with occupancy 0.5 are shown as small open circles.

nitrogens are donating a hydrogen bond each (via H1Na and H2Na) to the same acceptor (O12). The water molecule acting as ligand also donates two hydrogen bonds to the acceptors O7 and O14.

The framework is "interrupted" not only by a pendant phosphate oxygen but also by a zinc tetrahedron having a

(21) Ayi, A. A.; Neeraj, S.; Choudhury, A.; Natarajan, S.; Rao, C. N. R. *J. Phys. Chem. Solids* **2001**, *62*, 1481.

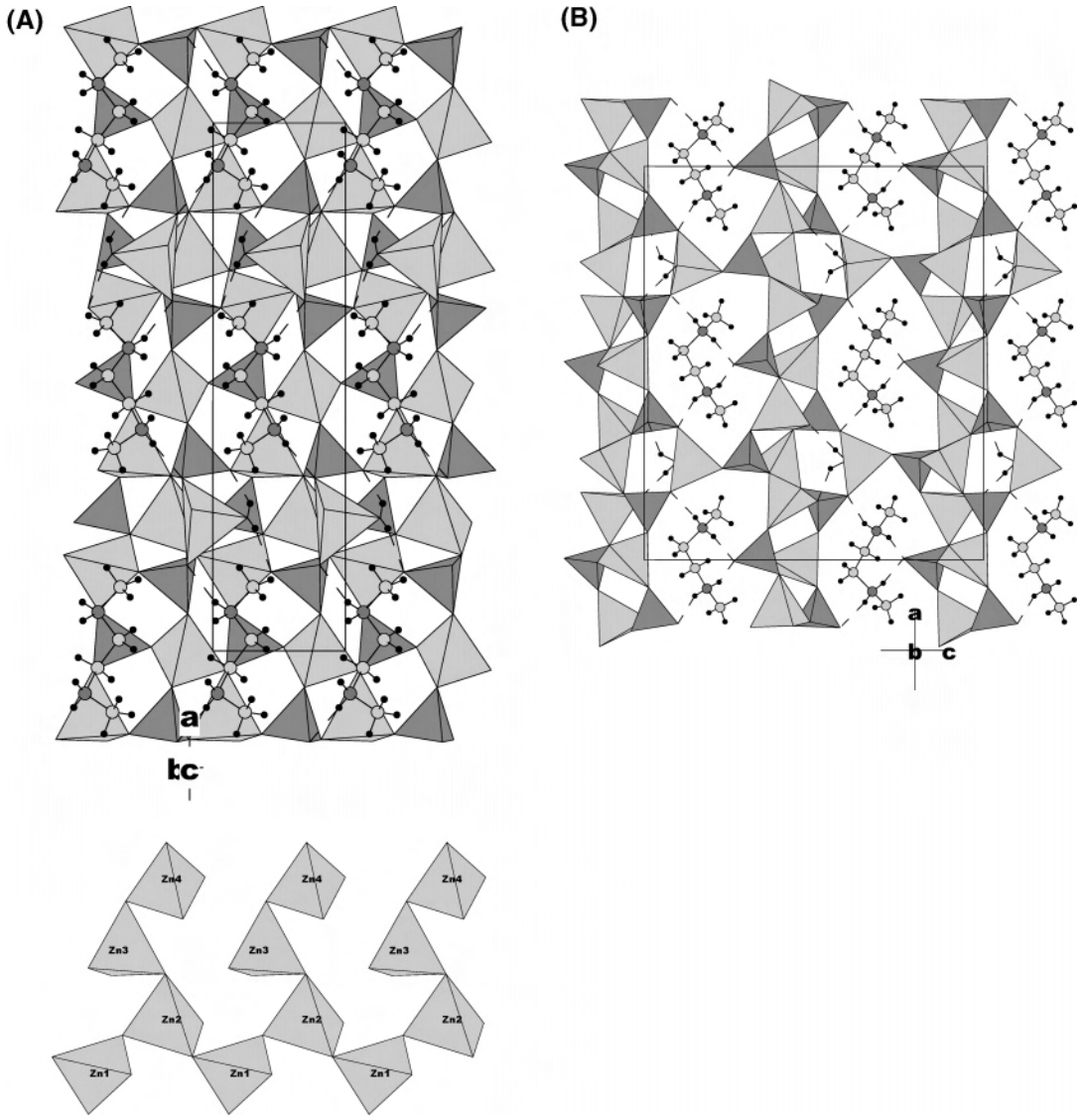

Figure 5. The crystal structure of $[C_4N_2H_{14}][Zn_5(H_2O)(PO_4)_4]$, **AU-III**. (A) Condensed nets formed by corner-sharing ZnO_4 and PO_4 tetrahedra of the inorganic moiety visible in the *a*,*b*-projection with chains of Zn1 and Zn2 tetrahedra with pendant Zn3 and Zn4 tetrahedra running in the *b*-direction shown below. (B) This *a*,*c*-projection showing one-dimensional 10-ring channels with the protonated template. ZnO_4 are light and PO_4 are dark tetrahedra, C and N are light and dark gray circles, respectively, and hydrogen are small size black circles.

water oxygen as a corner. The framework density, ρ_T, is used to describe how porous zeolite materials are, by the number of tetrahedra atoms, *T*, in the framework per 1000 Å^3. Open structured materials have less than ca. 21 framework tetrahedra per 1000 Å^3.[11a] The material **AU-III**, with T = P and Zn, has a framework density of $\rho_T = 18.8\ T/1000$ Å^3.

The solid-state ^{31}P CP/MAS NMR spectra acquired for **AU-III** at two different spinning frequencies (1800 and 4000 Hz) are displayed in Figure 6, and each show four distinct ^{31}P resonances in accordance with the four different phosphorus positions in the asymmetric unit. Iterative fitting and the simulations corresponding to the optimized parameters (Table 2) for these spectra are shown in Figure 6b and 6d. Excellent agreement between the experimental and simulated spectra is observed for the optimized parameters determined (Table 2). We note that the constant small difference in δ_{iso} of about 0.27 ppm is most likely related to a temperature dependence of δ_{iso} for either the external reference or the solid **AU-III** sample itself caused by frictional heating.[22]

Comparison with Related Materials. The structural motif formed by the inorganic part of the three new materials investigated in this work, **AU-I** to **III**, can be viewed as chainlike, layered, and framework, that is, increasing structural dimensionality, 1-D to 3-D. These materials are prepared from the same reaction mixture, and the structural dimensionality increases with the synthesis temperature. This is a consequence of the general thermodynamical metastability of nanoporous materials; that is, the lattice energy of the structure increases with increasing density, which is 1.894, 2.278, and 2.805 g/cm^3 for the series **AU-I** to **-III**, respectively.

The syntheses presented here can be compared to previous work. The materials α- and β-$LiZnPO_4 \cdot H_2O$ can be prepared from the same reaction mixture as microcrystalline powder or as larger crystals, respectively.[23] This was proposed to be caused by the different time scales of nucleation and crystal

(22) Bjørholm, T.; Jakobsen, H. J. *J. Magn. Reson*. **1989**, *84*, 204.

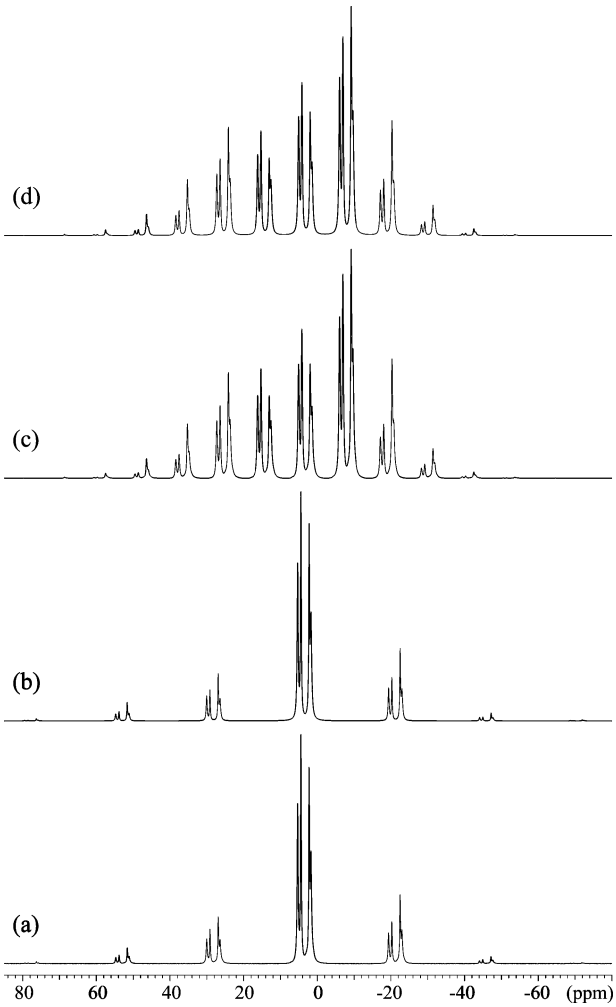

Figure 6. Experimental (a) and (c) and simulated ^{31}P CP/MAS NMR spectra (9.4 T, 161.8 MHz) of **AU-III** obtained using spinning speeds of $\nu_r = 4000$ Hz (a), (b) and $\nu_r = 1800$ Hz (c), (d). The experimental spectra were recorded using a relaxation delay of 16 s, 75 scans (a) and 2048 scans (c). The optimized simulations in (b) and (d) employ the ^{31}P CSA parameters listed in Table 2.

Table 2. ^{31}P Isotropic (δ_{iso}) and Anisotropic (δ_σ and η_σ) Chemical Shifts Parameters for **AU-III** $[C_4N_2H_{14}][Zn_5(H_2O)(PO_4)_4]$ As Determined from ^{31}P CP/MAS NMR Experiments at 9.4 T (161.8 MHz) and Two Different Spinning Speeds (ν_r)

site	ν_r (Hz)	δ_{iso}[a] (ppm)	δ_σ[b] (ppm)	η_σ[b] (ppm)
1	1800	5.06 ± 0.10	−34.9 ± 2.0	0.55 ± 0.05
1	4000	5.33 ± 0.10	−36.8 ± 2.0	0.56 ± 0.05
2	1800	4.16 ± 0.10	−34.4 ± 2.0	0.56 ± 0.10
2	4000	4.44 ± 0.10	−35.5 ± 2.0	0.41 ± 0.08
3	1800	1.93 ± 0.10	−45.0 ± 2.0	0.44 ± 0.05
3	4000	2.20 ± 0.10	−47.0 ± 2.0	0.44 ± 0.05
4	1800	1.44 ± 0.10	−40.8 ± 2.0	0.58 ± 0.05
4	4000	1.70 ± 0.10	−42.1 ± 2.0	0.52 ± 0.05

[a] Isotropic chemical shifts are relative to an external sample of 85% H_3PO_4. [b] The definition of the anisotropic chemical shift parameters is given in eq 1.

growth for α- and β-$LiZnPO_4 \cdot H_2O$; that is, the α-form crystallizes within some hours as micrometer scale crystallites, whereas the β-phase grows to millimeter-sized crystals within weeks or months. Furthermore, the density of the β-phase is slightly higher than that for α, so the existence of α- is due to faster kinetics rather than thermodynamic stability.[23a] In this respect, the precursor phase observed here resembles α-$LiZnPO_4 \cdot H_2O$ (only obtained as a white microcrystalline powder), and **AU-I** and **II** resemble the β-phase, which forms as larger crystals.

The reaction mechanism leading to the new materials **AU-I** and **II** is solution mediated observed by visual inspection of the reaction container. This is in contrast to a building-up process proposed by structural relationships identified between different amine-templated zinc phosphates. Hydrothermal treatment experiments also showed that some low dimensional zinc phosphates transform to other phases with higher structural dimensionality.[24] In this case, there is no direct structural relationship between the structures of **AU-I** to **-III**.

The fact that the structures are quite different for the series **AU-I** to **-III**, that is, 1D to 3D, is also reflected in the hydrogen-bond scheme. In the triclinic, 1D, structure, the greatest complexity is observed. The materials, **AU-I** to **-III**, all have diprotonated amines in the structures, but the phosphates have a different number of protons. In the 2D structure, the two phosphorus groups have 1 half (H1O) and 2 fully (H6O) occupied hydrogen positions. On average, the same HPO_4 is used for **AU-II** as for **I**. A hydrogen shared between two phosphates as found in **AU-II** is rare but has also been observed in the structure of $[C_4N_2H_{12}][Co_{0.14}Zn_{1.86}(PO_4)(H_{1.5}PO_4)_2]$.[25] There is no direct correlation between the pH of the reaction mixture and the number of protons associated with the phosphate groups, for example, $[C_2H_{10}N_2][Zn(HPO_4)_2]$ and $[C_2H_{10}N_2][Zn_2(H_2PO_4)_2(HPO_4)_2]$ prepared at pH 2−3 from the same reaction mixture at RT.[26] There might be a tendency for fewer hydrogen bonds with increasing temperature of the synthesis, that is, increasing density and phosphate groups with less hydrogen atoms, as found for $[C_3H_{12}N_2][Zn_2(HPO_4)_2(H_2PO_4)_2]$ and $[C_3H_{12}N_2][Zn(HPO_4)_2$ prepared from the same reaction mixture at 95 and 160 °C, respectively.[27]

The structures of **AU-I** to **AU-III** are compared to another family of zinc phosphates each prepared with the same structure-directing agent; see Table 3. The compounds are ordered with increasing structural dimensionality, *D*. The inorganic fraction of the materials is increasing with increasing *D*, expressed as the ratio polyhedra/amines, that is, the inorganic moiety relative to the organic moiety. The more dense is the material, that is, the higher *D*, the more zinc is present in the structure. The ratio P/(P−OH, P═O) estimates the degree of hydrogen bonding; that is, a value of 0.5 as found for the chainlike structures ($D = 1$) shows that the phosphate groups on average have two corners participating in hydrogen bonding. Therefore, as noted earlier, the density

(23) (a) Jensen, T. R. *J. Chem. Soc., Dalton Trans.* **1998**, *13*, 2261. (b) Harrison, W. T. A.; Gier, T. E.; Nicol, J. M.; Stucky, G. D. *J. Solid State Chem.* **1995**, *114*, 249.

(24) (a) Choudhury, A. *J. Mater. Chem.* **2001**, *11*, 1537. (b) Ayi, A. A. *J. Mater. Chem.* **2001**, *11*, 1181.

(25) Chen, X.; Zhao, Y.; Wnag, R.; Li, M.; Mai, Z. *J. Chem. Soc., Dalton Trans.* **2002**, 3092.

(26) Chidambaram, D.; Neeraj, S.; Natarajan, S.; Rao, C. N. R. *J. Solid State Chem.* **1999**, *147*, 154.

(27) Harrison, W. T. A.; Bircsak, Z.; Hannooman, L.; Zhang, Z. *J. Solid State Chem.* **1998**, *136*, 93.

Table 3. Two Families of Zinc Phosphates Each Prepared with the Same Amines as Template[a]

material	polyhedra/amines	Zn/P	P/(P−OH, P═O)	*D*	ref
$[C_4N_2H_{14}][Zn(HPO_4)_2]\cdot H_2O$, **AU-I**	3/1	1/2	2/(2+2)	1	*b*
$[C_4N_2H_{14}][Zn_2(H_{0.5}PO_4)_2(H_2PO_4)]$, **AU-II**	5/1	2/3	3/(3+0)	2	*b*
$[C_4N_2H_{14}][Zn_5(H_2O)(PO_4)_4]$, **AU-III**	9/1	5/4	4/(0+1)	3	*b*
$[C_6N_4H_{22}]_{0.5}[Zn(HPO_4)_2]$	3/0.5	1/2	2/(2+2)	1	28
$[C_6N_4H_{22}]_{0.5}[Zn_2(HPO_4)_3]$	5/0.5	2/3	3/(3+1)	2	28
$[C_6N_4H_{22}]_{0.5}[Zn_2(PO_4)_2]$	4/0.5	2/2	2/(0+1)	3	28
$[C_6N_4H_{22}]_{0.5}[Zn_3(PO_4)_2(HPO_4)]$	9/0.5	3/3	3/(1+1)	3	28
$[C_6N_4H_{22}]_{0.5}[Zn_4(PO_4)_3]$[c]	7/0.5	4/3	3/(0+0)	3	28

[a] Structural description from the content of the asymmetric units. The ratio between the organic and inorganic moiety is described by the ratio of polyhedra relative to amine molecules in the structure (polyhedra/amines). The dimensionality of the framework is denoted *D*, and the ratio P/(P−OH, P═O) describes the participation in hydrogen bonding. [b] This work. [c] The amine nitrogen is acting as ligand, forming ZnO_3N tetrahedra.

of such materials will also increase with the ratio polyhedra/amines and with *D*.

Conclusion

In the literature, there are some examples where two structurally different amine-templated zinc phosphates crystallized from the same reaction mixture treated at different temperatures.[29] This study appears to be the first example where one reaction mixture treated at different temperatures provides three new compounds, $[C_4N_2H_{14}][Zn(HPO_4)_2]\cdot H_2O$, **AU-I**, $[C_4N_2H_{14}][Zn_2(H_{0.5}PO_4)_2(H_2PO_4)]$, **AU-II**, and $[C_4N_2H_{14}][Zn_5(H_2O)(PO_4)_4]$, **AU-III**; see Table 4. These three materials are built from corner-sharing ZnO_4 and PO_4 tetrahedra forming chains, layers, or framework structures for **AU-I** to **-III**, respectively, and linked together by hydrogen bonds via diprotonated amine ions. The complete hydrogen-bond scheme is resolved for these new compounds and reveals some interesting phenomena, for example, a hydrogen shared between two phosphate groups in **AU-II** forming $H_{0.5}PO_4$ groups. Furthermore, the water molecules are different; that is, in **AU-I** it acts as hydrogen-bond donor and acceptor, whereas it acts as ligand in **AU-III** and coordinates to Zn. The reactions leading to the new materials **AU-I** and **-II** are solution mediated as observed by visual inspection of the reaction container. This work provides an example of the general metastability of nanoporous materials, resumed in Table 4. These materials are usually prepared under mild conditions. We observe here that the structural dimensionality/density of the materials, **AU-I** to **AU-III**, increases with the temperature of the synthesis.

Table 4. Synthesis and Structural Information on **AU-I** to **AU-III**

	AU-I	**AU-II**	**AU-III**
$T_{synthesis}$ (°C)	20	60	170
$t_{crystallization}$ (weeks)	∼6	∼2	∼0.3
dimensionality	1D	2D	3D
space group	$P\bar{1}$	$P2/n$	$Pna2_1$
ρ (g/cm^3)	1.89	2.28	2.81

Acknowledgment. The Siemens SMART diffractometer at the Department of Chemistry, University of Aarhus, is partly financed by Carlsberg fondet. T.R.J. thanks the Danish National Research Council for a Steno Stipend. The use of the facilities at the Instrument Centre for Solid-State NMR Spectroscopy, University of Aarhus, sponsored by the Danish Natural Science Research Council, Teknologistyrelsen, Carlsbergfondet, and Direktør Ib Henriksen Fond, is acknowledged.

Supporting Information Available: Powder X-ray diffraction (PXD) patterns and data from thermogravimetric (TG) measurements, Figures S1 and S2, respectively. Crystallographic information files (CIF) for the three compounds. This material is available free of charge via the Internet at http://pubs.acs.org.

IC049156G

(28) Choudhury, A.; Natarajan, S.; Rao, C. N. R. *Inorg. Chem.* **2000**, *39*, 4295.
(29) (a) Harrison, W. T. A.; Nenoff, T. M.; Eddy, M. M.; Martin, T. E.; Gier, T. E.; Stucky, G. D. *J. Mater. Chem.* **1992**, *2*, 1127. (b) See ref 27.